MARGINAL NOTES ON MAGNETOTELLURICS

M.N. BERDICHEVSKY
Moscow State University, 119899 Moscow Vorob'evy gory MGU Geological Department
(E-mail: berd@geo.geol.msu.su)

Abstract. The paper presents the brief notes on some questionable points of modern magnetotellurics. These controversial points are: (1) nature and structure of the magnetotelluric impedance tensor, (2) magnetotelluric dispersion relations, (3) the magnetotelluric eigenstate problem, (4) separation of local and regional effects (the local-regional decomposition), (5) sensitivity of the TM and TE modes of the two-dimensional field, (6) robustness of the TM and TE modes, (7) identification and correction of the static shift, and (8) strategy of the two-dimensional interpretation: unimodal or bimodal inversion? Consideration of all these topics gives a better insight into problems and potentialities of magnetotellurics.

Keywords: bimodal inversion, dispersion relation, eigenstate problem, impedance tensor, magnetotelluric sounding, tipper

1. Introduction

Nature and structure of the magnetotelluric impedance tensor, its general properties and geophysical informativeness, and methods of its analysis and interpretations are still at the centre of theoretical and methodological controversies in the world geoelectrical community. In this paper I would like to present some viewpoints that are characteristic of the Russian magnetotelluric school. The paper has the form of an overview consisting of brief (say, marginal) notes dedicated to eight points: (1) nature and structure of the magnetotelluric impedance tensor, (2) magnetotelluric dispersion relations, (3) magnetotelluric eigenstate problem, (4) separation of local and regional effects (the local-regional decomposition), (5) sensitivity of the TM and TE modes of the two-dimensional field, (6) robustness of the TM and TE modes, (7) identification and correction of the static shift, and (8) strategy of the two-dimensional interpretation: unimodal or bimodal inversion? I hope that these marginal notes can be interesting for my colleagues from the world geoelectrical community.

Surveys in Geophysics **20:** 341–375, 1999.
© 1999 *Kluwer Academic Publishers. Printed in the Netherlands.*

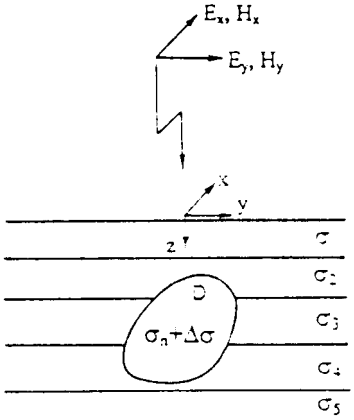

Figure 1. A layered model with an inhomogeneous body excited by the plane electromagnetic wave.

2. On Deterministic Nature of the Magnetotelluric Impedance and the Tipper

The long-standing question on the existence, nature and structure of linear algebraic relations between components of the electromagnetic field of the Earth is a basic challenge of geoelectrics. Should we consider the magnetotelluric linear relationships as a postulate supported by statistics of observations? Or, more properly, can we turn to the common principles of classic electrodynamics and derive the linear relations directly from the Maxwell equations?

Recently, Berdichevsky and Dmitriev (1997) expressed the components of the MT impedance tensor and the tipper in terms of excessive currents excited within a 3D inhomogeneous body D. The model is shown in Figure 1. The primary field is supposed to be uniform in the area containing an inhomogeneous body. It has two degrees of freedom corresponding to two different polarizations. Solving Maxwell's equations, the following deterministic relations have been obtained at the Earth's surface $z = 0$:

$$\begin{aligned} E_x &= Z_{xx}H_x + Z_{xy}H_y, \\ E_y &= Z_{yx}H_x + Z_{yy}H_y, \end{aligned} \tag{1}$$

where

$$Z_{xx} = \frac{J_x^{E2} - Z_n J_y^{H2} + (J_x^{E2}J_y^{H1} - J_x^{E1}J_y^{H2})}{1 + J_x^{H2} + J_y^{H1} + (J_x^{H2}J_y^{H1} - J_x^{H1}J_y^{H2})},$$

$$Z_{xy} = \frac{Z_n(1 + J_x^{H2}) + J_x^{E1} + (J_x^{E1}J_x^{H2} - J_x^{E2}J_x^{H1})}{1 + J_x^{H2} + J_y^{H1} + (J_x^{H2}J_y^{H1} - J_x^{H1}J_y^{H2})},$$

$$Z_{yx} = \frac{-Z_n(1 + J_y^{H1}) + J_y^{E2} + (J_y^{E2}J_y^{H1} - J_y^{E1}J_y^{H2})}{1 + J_x^{H2} + J_y^{H1} + (J_x^{H2}J_y^{H1} - J_x^{H1}J_y^{H2})},$$

$$Z_{yy} = \frac{J_y^{E1} + Z_n J_x^{H1} + (J_x^{E1} J_y^{H2} - J_x^{E2} J_y^{H1})}{1 + J_x^{H2} + J_y^{H1} + (J_x^{H2} J_y^{H1} - J_x^{H1} J_y^{H2})},$$

and

$$H_z = W_{zx} H_x + W_{zy} H_y, \tag{2}$$

where

$$W_{zx} = \frac{J_z^{H2} + (J_y^{H1} J_z^{H2} - J_y^{H2} J_z^{H1})}{1 + J_x^{H2} + J_y^{H1} + (J_x^{H2} J_y^{H1} - J_x^{H1} J_z^{H2})},$$

$$W_{zy} = \frac{J_z^{H1} + (J_x^{H2} J_z^{H1} - J_x^{H1} J_z^{H2})}{1 + J_x^{H2} + J_y^{H1} + (J_x^{H2} J_y^{H1} - J_x^{H1} J_z^{H2})}.$$

Here Z_n is the normal impedance observed in the absence of the inhomogeneous body and

$$\mathbf{J}^{Fp}(\mathbf{r}) = \int\int\int_D [\mathbf{G}^F(\mathbf{r}|\mathbf{r}_v)]\mathbf{j}^{(p)}(\mathbf{r}_v)\mathrm{d}V$$

$$F(\text{field}) = E, H \qquad p(\text{polarization}) = 1, 2$$

is the convolution of excessive currents j with Green's tensor $[G]$.

Thus,

$$\begin{aligned} \mathbf{E}_\tau &= [\mathbf{Z}]\mathbf{H}_\tau, \\ H_z &= [\mathbf{W}]\mathbf{H}_\tau, \end{aligned} \tag{3}$$

where

$$\mathbf{E}_\tau = \begin{bmatrix} E_x \\ E_y \end{bmatrix} \qquad \mathbf{H}_\tau = \begin{bmatrix} H_x \\ H_y \end{bmatrix}$$

are the horizontal components of the electromagnetic field and

$$[\mathbf{Z}] = \begin{bmatrix} Z_{xx} & Z_{xy} \\ Z_{yx} & Z_{yy} \end{bmatrix} \qquad [\mathbf{W}] = [W_{zx} \quad W_{zy}]$$

are the impedance tensor and the tipper.

These formulae give a *deterministic basis* for examining the properties of the MT transfer functions. For instance, we see that the off-diagonal components of the MT impedance contain the basic information on vertical resistivity profile, while its diagonal components and the components of the tipper reflect mainly the lateral effects. With this understanding, we can assess the expedience of apparent resistivity

representations. In the 1D model the transformation of the impedance into apparent resistivity yields a vivid qualitative picture of vertical geoelectrical cross-section. This useful property of the one-dimensional impedance is inherited by off-diagonal components Z_{xy}, Z_{yx} of the impedance tensor (though with some distortion), and hardly by its diagonal components Z_{xx}, Z_{yy}, which more likely characterize the geoelectrical asymmetry of the Earth. So, it would appear reasonable to calculate the apparent resistivity of a horizontally inhomogeneous medium as

$$\rho_{xy} = \frac{|Z_{xy}|^2}{\omega\mu_0}, \qquad \rho_{yx} = \frac{|Z_{yx}|^2}{\omega\mu_0}. \tag{4}$$

All these relations still stand if the atmosphere has nonzero conductivity and the displacement currents are taken into account.

Similar relations may be observed in the models with three degrees of freedom of the primary field. Let us consider the uniform primary field that can be polarized in any of three orthogonal directions. In this case,

$$E_x = Z_{xx}H_x + Z_{xy}H_y + Z_{xz}H_z,$$

$$E_y = Z_{yx}H_x + Z_{yy}H_y + Z_{yz}H_z,$$

$$E_z = Z_{zx}H_x + Z_{zy}H_y + Z_{zz}H_z.$$

Now neglect the atmosphere conductivity and assume that over a wide range of low frequencies we can disregard the displacement currents (not too severe assumptions). Then we can say that the conductive Earth comes into contact with nonconductive air and at the lower side of the Earth's surface $E_z(z = 0 +) = 0$ (no telluric leakage through the Earth's surface). Hence,

$$H_z = \tilde{W}_{zx}H_x + \tilde{W}_{zy}H_y$$

and

$$E_x = \tilde{Z}_{xx}H_x + \tilde{Z}_{xy}H_y,$$

$$E_y = \tilde{Z}_{yx}H_x + \tilde{Z}_{yy}H_y,$$

where

$$\tilde{W}_{zx} = -\frac{Z_{zx}(+0)}{Z_{zz}(+0)}, \qquad \tilde{W}_{zy} = -\frac{Z_{zy}(+0)}{Z_{zz}(+0)}$$

and

$$\tilde{Z}_{xx} = Z_{xx} + \tilde{W}_{zx}Z_{xz},$$

$$\tilde{Z}_{xy} = Z_{xy} + \tilde{W}_{zy} Z_{xz},$$

$$\tilde{Z}_{yx} = Z_{yx} + \tilde{W}_{zx} Z_{yz},$$

$$\tilde{Z}_{yy} = Z_{yy} + \tilde{W}_{zy} Z_{yz}.$$

Thus, in the models under consideration, *the tipper and the impedance tensor have matrices of dimension* 1×2 *and* 2×2 *no matter what is the number of degrees of freedom in the primary fields.*

3. On the Magnetotelluric Dispersion Relations

In magnetotellurics, the Kramers–Kronig dispersion relations of two kinds are considered: (1) between real and imaginary parts of the impedance Z, (2) between apparent resistivities $\rho_A = |Z|^2/\mathrm{i}\omega\mu_0$ and impedance phases $\varphi = \arg Z$ (Weidelt 1972).

The dispersion relations of the first kind take the form:

$$R(\omega_0) = \frac{2}{\pi} pv \int_0^\infty \frac{X(\omega)}{\omega^2 - \omega_0^2} \omega \mathrm{d}\omega,$$

$$X(\omega_0) = -\frac{2\omega_0}{\pi} pv \int_0^\infty \frac{R(\omega)}{\omega^2 - \omega_0^2} \mathrm{d}\omega, \tag{5}$$

where pv means that integral is taken in the sense of the Cauchy principal value, and $R = \mathrm{Re}(Z/\mathrm{i}\omega\mu_0)$, $X = \mathrm{Im}(Z/\mathrm{i}\omega\mu_0)$. These relations exist if the impedance Z has no poles in the upper half-plane of the complex frequency $\Omega = \omega + \mathrm{i}\lambda$. Here and below the complex time-factor is $\mathrm{e}^{-\mathrm{i}\Omega\mu_0}$.

The dispersion relations of the second kind are in the form:

$$\varphi(\omega_0) = -\frac{\pi}{4} - \frac{\omega_0}{\pi} pv \int_0^\infty \ln \rho_A(\omega) \frac{\mathrm{d}\omega}{\omega^2 - \omega_0^2},$$

$$\ln \frac{\rho_A(\omega_0)}{\rho_A(\infty)} = \frac{4}{\pi} pv \int_0^\infty \left[\frac{\pi}{4} + \varphi(\omega)\right] \frac{\omega \mathrm{d}\omega}{\omega^2 - \omega_0^2}, \tag{6}$$

where $\rho_A(\infty)$ is the high-frequency asymptotic value of the apparent resistivity. These relations exist if the impedance Z satisfies the condition of the minimum phase, i.e., if it has neither poles nor zeros in the upper half-plane of the complex frequency Ω.

The existence of the dispersion relations is among the most controversial subjects of today's magnetotellurics.

Weidelt (1972) and Weidelt and Kaikkonen (1994) gave rigorous proof to the validity of the dispersion relations of both kinds in the classes of 1D and B-polarized 2D models.

Yee and Paulson (1988) considered the impedance tensor of the heterogeneous Earth as a linear casual operator and on this ground state that the dispersion relations of both kinds hold good in all models, including 3D ones. But this consideration is vulnerable to criticism since the electrical and magnetic fields interact with each other and we hardly can say that one of these fields is a cause and another is an effect (Svetov 1991). *The magnetelluric system is casual in the sense that the electrical and magnetic fields are effects of the same cause, for instance, of ionospheric or magnetospheric currents.*

Many people are involved in this discussion (Fischer and Schnegg 1980, 1993; Egbert 1990; Svetov 1991; Berdichevsky and Pokhotelov 1997a,b). Nowadays it is evident that we have to leave room for the possibility of violation of dispersion relations in the classes of E-polarized 2D models and 3D models. The discussion makes a clear practical sense: if the Kramers-Kronig relations are violated, our philosophy of amplitude-phase inversion of MT-data should be revised. This is seen from the following example. Take a regional elongated (quasi 2D) depression with local near-surface 3D inhomogeneities that violate the dispersion relations. Here the separate inversions of transverse apparent resistivity and phase curves in the class of B-polarized 2D models may yield conflicting geoelectrical structures (even with static shift corrections).

Meantime the magnetotelluric observations give a good deal of examples with dramatic violation of MT dispersion relations. Figure 2 presents apparent resistivity and phase curves obtained in the mountains of the Lesser Caucasus. Here the accuracy of the phase measurements seems to be rather high (good spatial correlation!), but the difference between observed and calculated φ-curves amounts up to 35°.

In an attempt to understand these phenomena, Berdichevsky and Pokhotelov (1997b) constructed a 2D + 3D superposition model where the Kramers-Kronig relations were violated (Figure 3, model A). The model contains a two-dimensional deep conductive prism R of width $2\Delta y$ and a three-dimensional shallow resistive cylinder L of radius a ($a \ll \Delta y$). The calculations have been carried out by an approximate hybrid method suggested by Berdichevsky and Dmitriev (1976). They consisted of 4 stages: (1) solution of the 2D problem for R using the numerical method of Wannamaker et al. (1987) and determination of the 2D impedance

$$[\mathbf{Z}^{2D}] = \begin{bmatrix} 0 & Z_{xy}^{2D} \\ Z_{yx}^{2D} & 0 \end{bmatrix}, \tag{7}$$

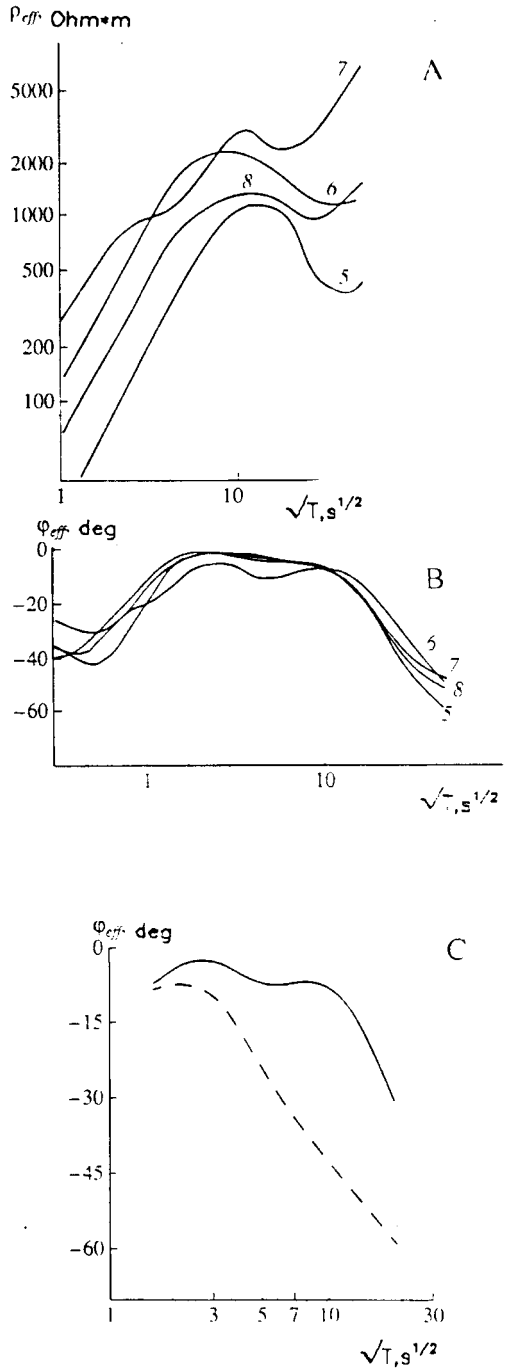

Figure 2. Magnetotelluric curves for the Armenian Upland. (A, B) Apparent resistivities and impedance phases; digits at the curves are the numbers of MT-sounding sites. (C) Violation of the dispersion relations in MTS-6; the solid line is the observed phase curve, and the dashed line is the phase curve calculated from the apparent resistivity curve; taken from Berdichevsky and Pokhotelov (1997b).

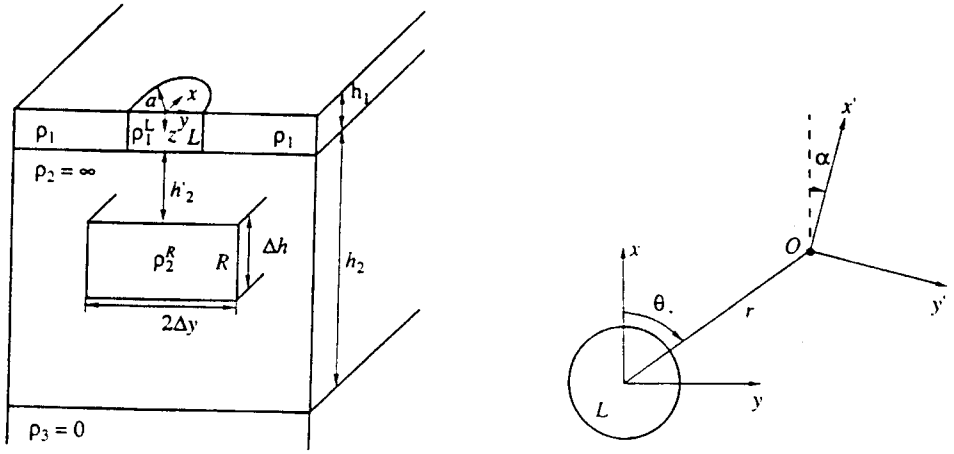

Figure 3. Superposition of near-surface cylindrical (L) and deep prismatic (R) structures. Model A: (ρ_1 = 10 Ohm.m, h_1 = 0.5 km, $\rho_1^L = \infty$, a = 0.125 km, $\rho_2 = \infty$, h_2 = 80 km, ρ_2^R = 10 Ohm.m, h'_2 = 10 km, Δh = 10 km, Δy = 20 km, ρ_3 = 0. Observation site O: θ = 45°, r = 0.129 km, α = 50°. Model B: ρ_1 = 100 Ohm.m, h_1 = 0.1 km, ρ_1^L = 10 Ohm.m, a = 0.1 km, $\rho_2 = \infty$, h_2 = 100 km, ρ_2^R = 10 Ohm.m, h'_2 = 10 km, Δh = 10 km, Δy = 100 km, ρ_3 = 0.01 Ohm.m. Observation site O: θ = 45°, r = 0.11 km, α = 45°.

where Z_{xy}^{2D} and Z_{yx}^{2D} relate to the TE and TM modes; (2) solution of the 3D problem for L using the quasi-static analytical thin-sheet approximation of Berdichevsky and Dmitriev (1976) and determination of the electrical distortion matrix

$$[\mathbf{e}] = \begin{bmatrix} e_{xx} & e_{xy} \\ e_{yx} & e_{yy} \end{bmatrix} \tag{8}$$

and the magnetic distortion matrix

$$[\mathbf{h}] = [\mathbf{I}] + 0.5[\mathbf{R}]\{S[\mathbf{e}] - S_1[\mathbf{I}]\}[Z^{2D}] = \begin{bmatrix} h_{xx} & h_{xy} \\ h_{yx} & h_{yy} \end{bmatrix}, \tag{9}$$

where

$$[\mathbf{I}] = \begin{bmatrix} 1 & 0 \\ 0 & 1 \end{bmatrix}, \quad [\mathbf{R}] = \begin{bmatrix} 0 & -1 \\ 1 & 0 \end{bmatrix}, \quad S = \begin{cases} S_1^L = h_1/\rho_1^L & O \in L \\ S_1 = h_1/\rho_1 & O \notin L \end{cases};$$

(3) synthesis of the 2D and 3D problems and determination of the synthesized impedance:

$$[\mathbf{Z}] = [\mathbf{Z}^{2D+3D}] = [\mathbf{e}][\mathbf{Z}^{2D}][\mathbf{h}]^{-1} = \begin{bmatrix} Z_{xx} & Z_{xy} \\ Z_{yx} & Z_{yy} \end{bmatrix}; \tag{10}$$

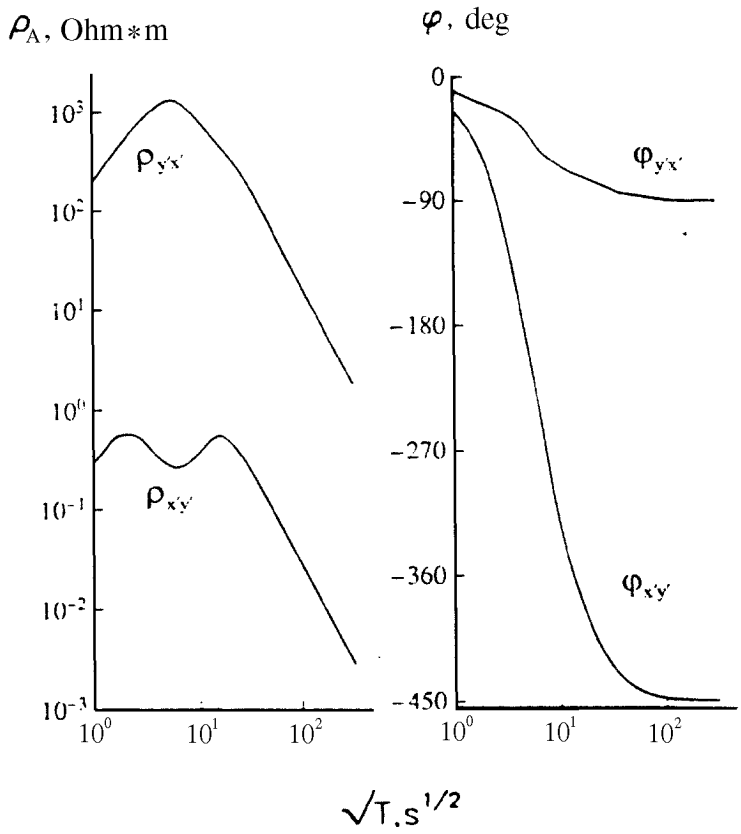

Figure 4. Curves of apparent resistivity and impedance phase at a site O ($\theta = 45°$, $r = 0.129$ km), the x'-axis is directed at angle $\alpha = 50°$.

and (4) rotation of the synthesized impedance through an angle α:

$$\begin{bmatrix} Z_{x'x'} & Z_{x'y'} \\ Z_{y'x'} & Z_{y'y'} \end{bmatrix} = \begin{bmatrix} \cos\alpha & \sin\alpha \\ -\sin\alpha & \cos\alpha \end{bmatrix} \begin{bmatrix} Z_{xx} & Z_{xy} \\ Z_{yx} & Z_{yy} \end{bmatrix} \begin{bmatrix} \cos\alpha & -\sin\alpha \\ \sin\alpha & \cos\alpha \end{bmatrix}. \tag{11}$$

Figure 4 demonstrates the $\rho_{x'y'}$ and $\varphi_{x'y'}$-curves obtained in the immediate vicinity of the cylinder, axis x' being almost normal to the cylinder. The Kramers–Kronig transforms of $\rho_{x'y'}$, $\varphi_{x'y'}$ and Re $Z_{x'y'}$, Im $Z_{x'y'}$ are displayed in Figure 5. We observe a strong violation of the dispersion relations between $\rho_{x'y'}$ and $\varphi_{x'y'}$, while Re $Z_{x'y'}$ and Im $Z_{x'y'}$ satisfy the dispersion relations with high accuracy. One can suppose that in the model under consideration there are zeros and no poles in the upper half-plane of complex frequency.

Calculations verify the reality of anomalous phenomena that are exhibited in violation of dispersion relations. At present we know less than nothing about these

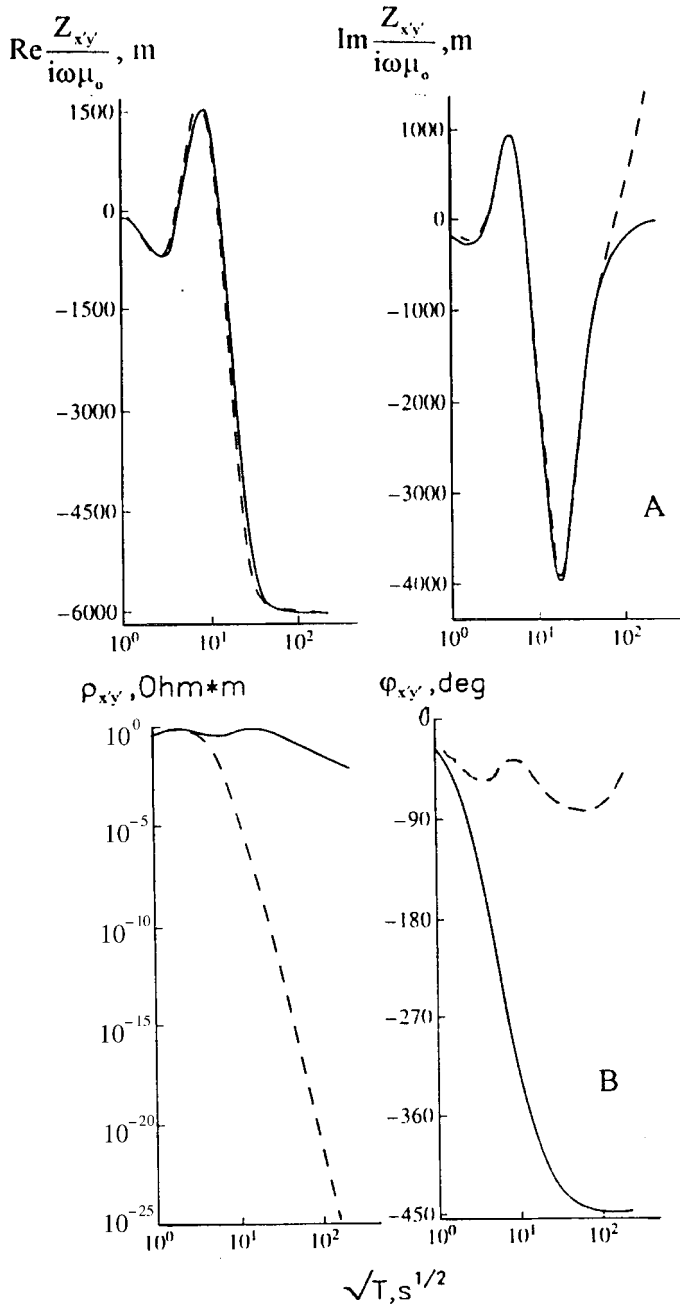

Figure 5. The Kramer–Kronig transformation at a site O (θ = 45°, r = 0.129 km), the x'-axis is directed at angle α = 50°. (A) real and imaginary parts of the normalized impedance $Z_{x'y'}/i\omega\mu_0$, (B) apparent resistivity $\rho_{x'y'}$ and impedance phase $\varphi_{x'y'}$. Solid line – initial values, dashed line – values calculated with formulae (5) and (6); taken from Berdichevsky amd Pokhotelov (1997b).

phenomena. To fill the gap, we need experimental materials and theoretical developments. A starting point may be the including of special test controlling the dispersion relations into existing programs of MT data processing and inversion.

4. On the Magnetotelluric Eigenstate Problem

All the information inherent in the magnetotelluric impedance tensor can be systematized and concentrated on the optimum directions by the methods related to the eigenstate problem. The basic ideas about magnetotelluric eigenstate problem have been suggested by Swift (1967).

The two-dimensional model is the starting point. Let the x-axis coincide with the strike of the 2D model. Then the impedance tensor takes the form

$$[\mathbf{Z}] = \begin{bmatrix} 0 & Z_{xy} \\ Z_{yx} & 0 \end{bmatrix} = \begin{bmatrix} 0 & Z^{\parallel} \\ -Z^{\perp} & 0 \end{bmatrix} \tag{12}$$

whence

$$E_x = Z^{\parallel} H_y, \quad E_y = -Z^{\perp} H_x, \tag{13}$$

where $Z^{\parallel} = Z_{xy}$ and $Z^{\perp} = -Z_{yx}$ are the longitudinal and transverse components of the tensor $[\mathbf{Z}]$ oriented along the strike and perpendicularly to the strike. It is natural to consider the values of $Z^{\parallel}$ and $Z^{\perp}$ as the *principal values* (eigenvalues) and the longitudinal and transverse directions as the *principal directions* (eigendirections) of the magnetotelluric impedance tensor. In this context, the fields $\mathbf{E}_{\tau}$ and $\mathbf{H}_{\tau}$ linearly polarized in the longitudinal and transverse directions manifest themselves as the *eigenfields* of the magnetotelluric impedance tensor. The two-dimensional tensor $[\mathbf{Z}]$ has two pairs of the eigenfields:

$$\mathbf{E}_{\tau}^{(1)} = \begin{bmatrix} E_x^{(1)} \\ 0 \end{bmatrix}, \quad \mathbf{H}_{\tau}^{(1)} = \begin{bmatrix} 0 \\ H_y^{(1)} \end{bmatrix} \quad \text{and} \quad \mathbf{E}_{\tau}^{(2)} = \begin{bmatrix} 0 \\ E_y^{(2)} \end{bmatrix}, \quad \mathbf{H}_{\tau}^{(2)} = \begin{bmatrix} H_x^{(2)} \\ 0 \end{bmatrix}. \tag{14}$$

In each pair the electric eigenfield is the transform of the magnetic eigenfield.

These representations exhibit 3 characteristic properties of the 2D magnetotelluric impedance tensor: (1) the impedance tensor reduced to its principal directions has zero diagonal, (2) the electric and magnetic vectors within each eigenfield pair are mutually perpendicular (*the E-H, E-H perpendicularity*), and (3) the electric vectors from different eigenfield pairs are mutually perpendicular, as well as magnetic vectors from different eigenfield pairs are mutually perpendicular (*the E-E, H-H perpendicularity*). This gives a clue to the generalization of the magnetotelluric eigenstate problem to the 3D model.

Nowadays three methods to solve the eigenstate problem are mostly used in the geoelectric community: (1) the rotation method (Swift, 1967; Sims and Bostick, 1967), (2) the orthogonalization method (Swift, 1967; Eggers, 1982), (3) the diagonalization method (Swift, 1967; LaTorraca, Madden and Korringa, 1986; Yee and Paulson 1987).

The rotation method is rather simple. It reduces to the tensor rotation which minimizes the matrix diagonal. Here the 3D tensor is approximated by the 2D tensor. The calculations result in determining the principal values $\zeta_1 = |\zeta_1|\ e^{i\xi_1}$, $\zeta_2 = |\zeta_2|\ e^{i\xi_2}$ and principal directions α_1, $\alpha_2 = \alpha_1 + \pi/2$ (α is an angle between the x-axis and the principal direction).

The orthogonalization and diagonalization methods reduce to the detection of the perpendicular eigenfields. The directions of the eigenfields are found as directions of the major axes of eigenfield polarization ellipses. In the orthogonalization method we look for the electrical and magnetic eigenfields with the E-H, E-H perpendicularity. This method is a modification of the classical eigenstate formulation. Here the calculations result in determining the principal values $\zeta_1 = |\zeta_1|\ e^{i\xi_1}$, $\zeta_2 = |\zeta_2|\ e^{i\xi_2}$ and principal directions $\alpha_1 = \alpha_{E_1}$, $\alpha_2 = \alpha_{E_2}$ (α_{E_1} and α_{E_2} are the directions of major axes of polarization ellipses for both electrical eigenfields). In the diagonalization method we look for the electrical and magnetic eigenfields with the E-E, H-H perpendicularity This method is a modification of the Lannczos SVD-formulation. Here the calculations result in determining the principal values $\zeta_1 = |\zeta_1|\ e^{i\xi_1}$, $\zeta_2 = |\zeta_2|\ e^{i\xi_2}$ and principal directions $\alpha_1 = \alpha_{E_1}$, $\alpha_2 = \alpha_{H_1}$ (α_{E_1} and α_{H_1} are the directions of major axes of polarization ellipses for the electrical and magnetic eigenfields respectively). Both methods offer *purely mathematical procedures* that attach some properties of the 2D model to the 3D model and the discussion about their physical meaning is a bit scholastic. The challenge is to find relations between eigenstate indications and properties of geoelectrical structures.

It would be instructive to examine some characteristic models and compare results received with all these methods. The model considered by Nguen Tkhan Van and me consisted of an Γ-shaped near-surface resistive inlier and a 2D deep conductive prism (Figure 6). The problem was solved by the hybrid method described in Section 2. The calculations have been carried out using the numerical methods of Wannamaker et al. (1987) for the 2D prism and Debabov (1980) for the L-shaped inclusion. The eigenstate estimations were done at 14 sites.

Figure 7 shows amplitudes $|\zeta|$ and phases ξ of the impedance principal values obtained by the rotation method (1), the orthogonalization method (2), and the diagonalization method (3). All three techniques give close principal values (the difference at many sites does not exceed 5% and 3° and only at a few sites amounts up to 12% and 6°). Here the distinctions between methods are rather small, but they vividly manifest themselves in the parameter

$$N = \left| \frac{\zeta_1 - \zeta_2}{\zeta_1 + \zeta_2} \right| \tag{15}$$

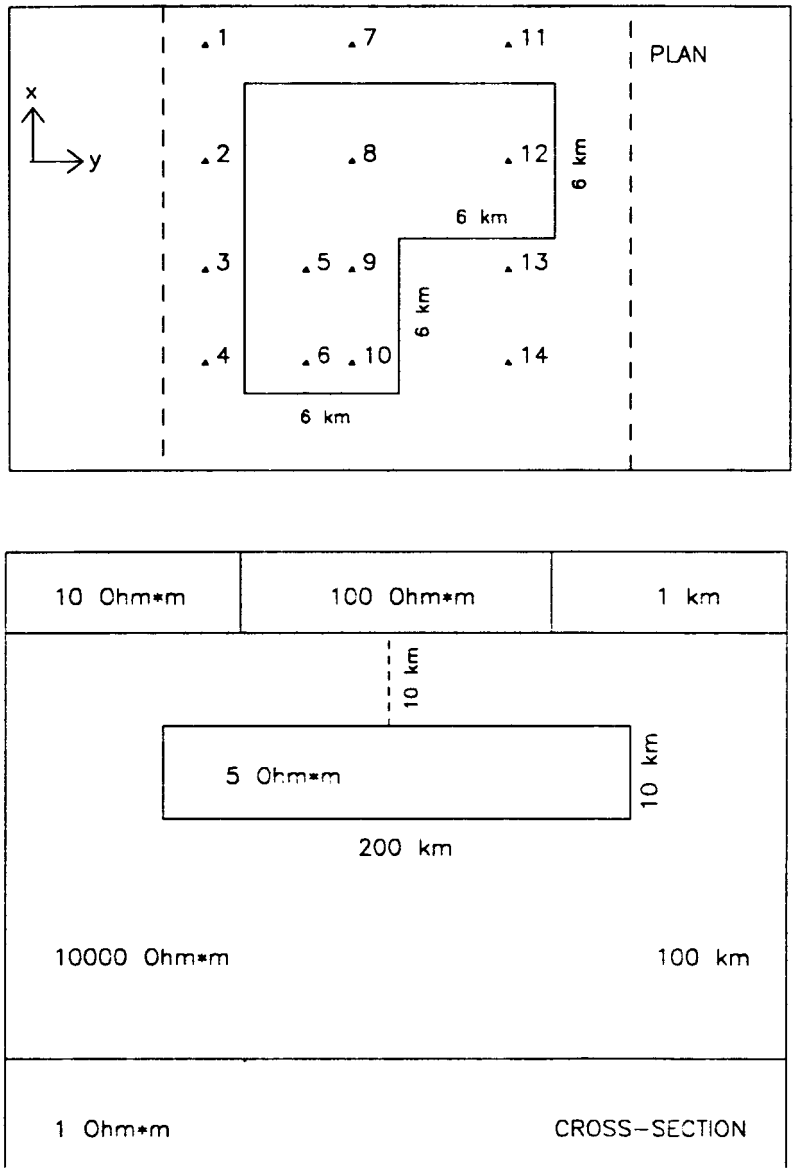

Figure 6. Model with an Γ-shaped near-surface resistive inlier and a 2D deep conductive prism. 1, 2, 3, . . . – observation sites.

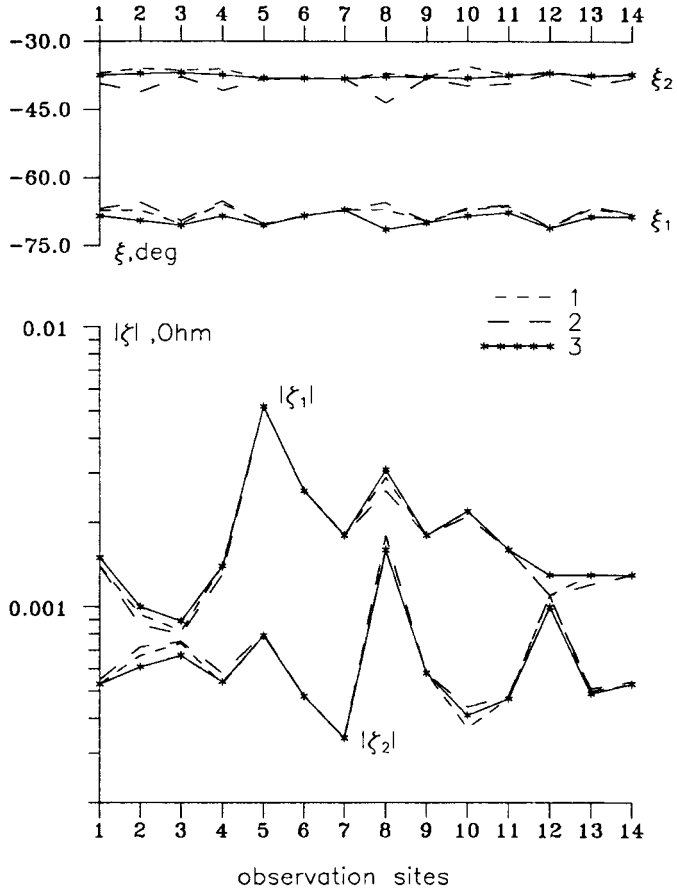

Figure 7. Principal values of the impedance tensor. 1 – rotation method, 2 – orthogonalization method, 3 – diagonalization method.

that reflects the lateral inhomogeneity (Figure 8). In 1D models we have $N = 0$. Deviation of N from zero indicates the lateral effects caused by 2D or 3D structures. In the model under consideration the diagonalization method gives the maximum N-values being the most sensitive to lateral effects.

Now look at Figure 9 which shows the impedance principal directions α obtained by three methods. Though the α-values are in close qualitative agreement, the difference between them may attain 15° and even 25°. Using α-values we can calculate the angular skew

$$S_a = \left| |\alpha_1 - \alpha_2| - \frac{\pi}{2} \right| \tag{16}$$

that reflects asymmetry of the medium. In 2D models and axisymmetric 3D models we have $S_a = 0$. Deviation of S_a from zero indicates the effect of an asymmetric 3D structure. In the model under consideration the orthogonalization method gives the

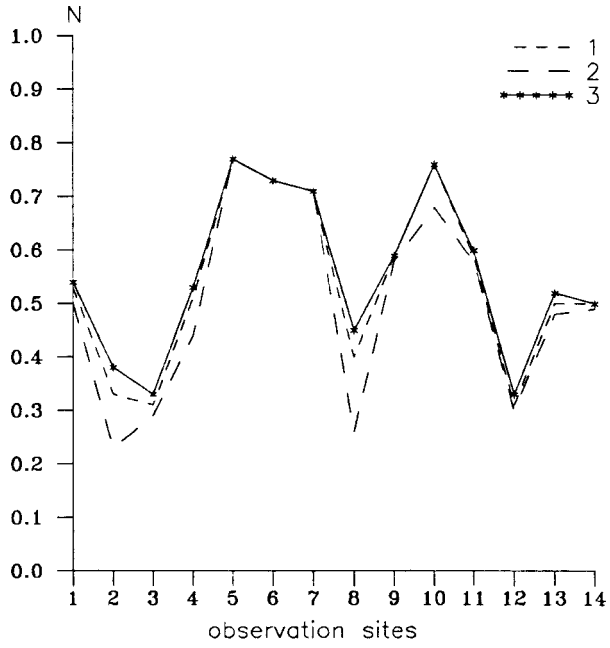

Figure 8. Parameter of inhomogeneity. 1 – rotation method, 2 – orthogonalization method, 3 – diagonalization method.

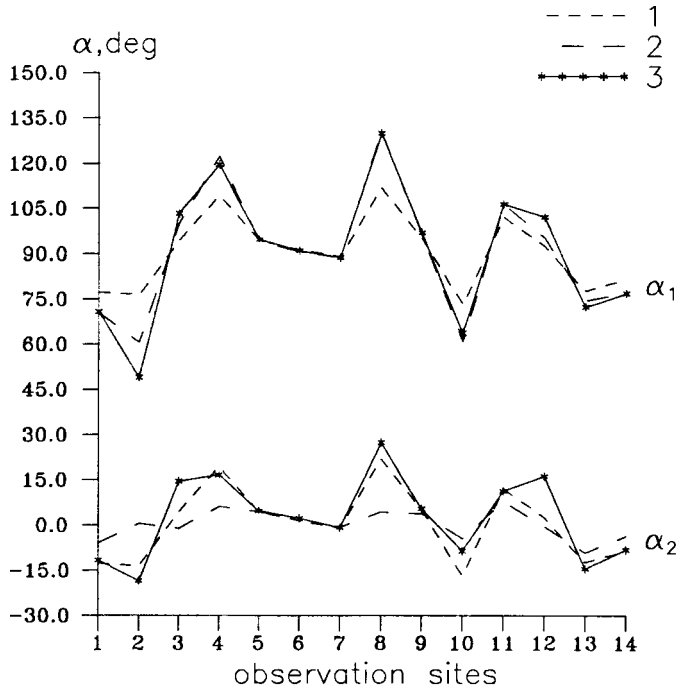

Figure 9. Principal directions of the impedance tensor. 1 – rotation method, 2 – orthogonalization method, 3 – diagonalization method.

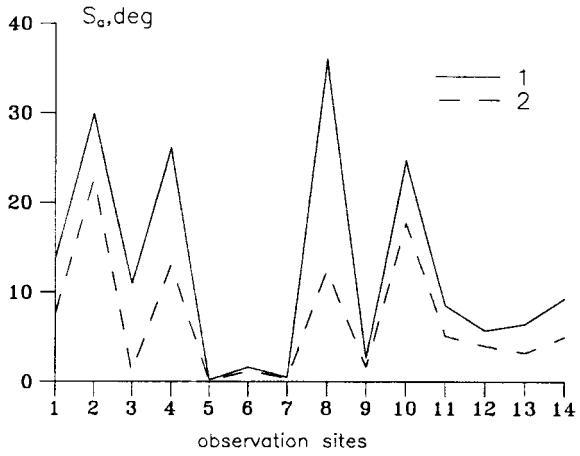

Figure 10. Angular skew. 1 – orthogonalization method, 2 – diagonalization method.

maximum S_a-values to be the most sensitive to the structural asymmetry (Figure 10).

The *orthogonalization and diagonalization methods complement each other* and are the most informative ones since they fill all 8 degrees of impedance freedom. What we would like to stress is that the orthogonalization method has an elegant theory and does not need any limitations, while the diagonalization method assumes that the Earth is locally passive and real part of Pointing's vector everywhere points down. This is a weak point of the diagonalization method because nobody has proved that near-surface local inhomogeneities cannot emit the energy back into the air.

5. On the Local-Regional Decomposition

For separation of local and regional effects we use decompositions of two kinds: (1) The Bahr decomposition (Bahr 1988), and (2) The Groom-Bailey decomposition (Groom and Bailey 1989). These quasi-static decompositions rest on the same model represented by superposition of 2D regional and 3D local structures.

The Bahr and Groom–Bailey decompositions have the same basis, but differ in technology.

Return to the 2D + 3D superposition model examined in Section 2. The basic representation for the local-regional decomposition can be derived directly from Equation (10). If local structure is sufficiently small and frequency is sufficiently low, we neglect the magnetic distortion

$$[\mathbf{h}] = \begin{bmatrix} h_{xx} & h_{xy} \\ h_{yx} & h_{yy} \end{bmatrix} \approx \begin{bmatrix} 1 & 0 \\ 0 & 1 \end{bmatrix} \tag{17}$$

and represent the local (synthesized) impedance tensor as a product of the real-valued electric distortion matrix and regional (two-dimensional) impedance tensor:

$$[\mathbf{Z}] \approx [\mathbf{e}][\mathbf{Z}^{2\mathrm{D}}] = \begin{bmatrix} e_{xx} & e_{xy} \\ e_{yx} & e_{yy} \end{bmatrix} \begin{bmatrix} Z_{xx}^{2\mathrm{D}} & Z_{xy}^{2\mathrm{D}} \\ Z_{yx}^{2\mathrm{D}} & Z_{yy}^{2\mathrm{D}} \end{bmatrix}$$

$$= \begin{bmatrix} e_{xx}Z_{xx}^{2\mathrm{D}} + e_{xy}Z_{yx}^{2\mathrm{D}} & e_{xx}Z_{xy}^{2\mathrm{D}} + e_{xy}Z_{yy}^{2\mathrm{D}} \\ e_{yx}Z_{xx}^{2\mathrm{D}} + e_{yy}Z_{yx}^{2\mathrm{D}} & e_{yx}Z_{xy}^{2\mathrm{D}} + e_{yy}Z_{yy}^{2\mathrm{D}} \end{bmatrix}. \tag{18}$$

In the Bahr decomposition we rotate the tensor [**Z**] and examine the phase relations between its components. The calculations result in determining the regional strike and phases of the principal values of the regional impedance.

The Groom–Bailey decomposition reduces to the least squares approximation of the tensor [**Z**] by the product of the special matrix [**e**] reflecting the twist and shear deformation of the electric field and the regional tensor [$\mathbf{Z}^{2\mathrm{D}}$]. The calculations result in determining the regional strike and phases of the principal values of the regional impedance as well as the twist and shear angles.

Here I would like to note that the *Bahr and Groom–Bailey decompositions give stable results if transverse and longitudinal components of the 2D regional impedance have significantly different phases.* If the phases do not differ, both decompositions are unusable since the Bahr equation for the strike reduces to zero over zero and the system of the Groom–Bailey equations becomes indeterminate.

Let us consider a model example (Figure 3, model B). Here a 3D local cylindrical resistive inlier L is superimposed on a regional 2D conductive prismatic structure R. The problem was solved by the hybrid method given in Section 2.

Figure 11 depicts the apparent resistivity and phase curves calculated from longitudinal and transverse components of the 2D regional impedance. Note that at T $\cong$ 7.5 s and T $>$ 40 000 s the phases of longitudinal and transverse impedances virtually coincide.

Consider some parameters, which characterize the superposition model.

The parameter

$$\Delta = |\mathrm{Arg}\, Z^{\parallel} - \mathrm{Arg}\, Z^{\perp}| = \cos^{-1} \frac{|\det[\mathrm{Re}\mathbf{Z}] + \det[\mathrm{Im}\mathbf{Z}]|}{|\det[\mathbf{Z}]|} \tag{19}$$

with

$$\det[\mathrm{Re}\mathbf{Z}] = \mathrm{Re}Z_{xx}\mathrm{Re}Z_{yy} - \mathrm{Re}Z_{xy}\mathrm{Re}Z_{yx},$$

$$\det[\mathrm{Im}\mathbf{Z}] = \mathrm{Im}Z_{xx}\mathrm{Im}Z_{yy} - \mathrm{Im}Z_{xy}\mathrm{Im}Z_{yx},$$

$$\det[\mathbf{Z}] = Z_{xx}Z_{yy} - Z_{xy}Z_{yx}$$

is the difference between longitudinal and transverse phases calculated directly from the local impedance tensor [**Z**] and its real and imaginary parts [Re **Z**], [Im

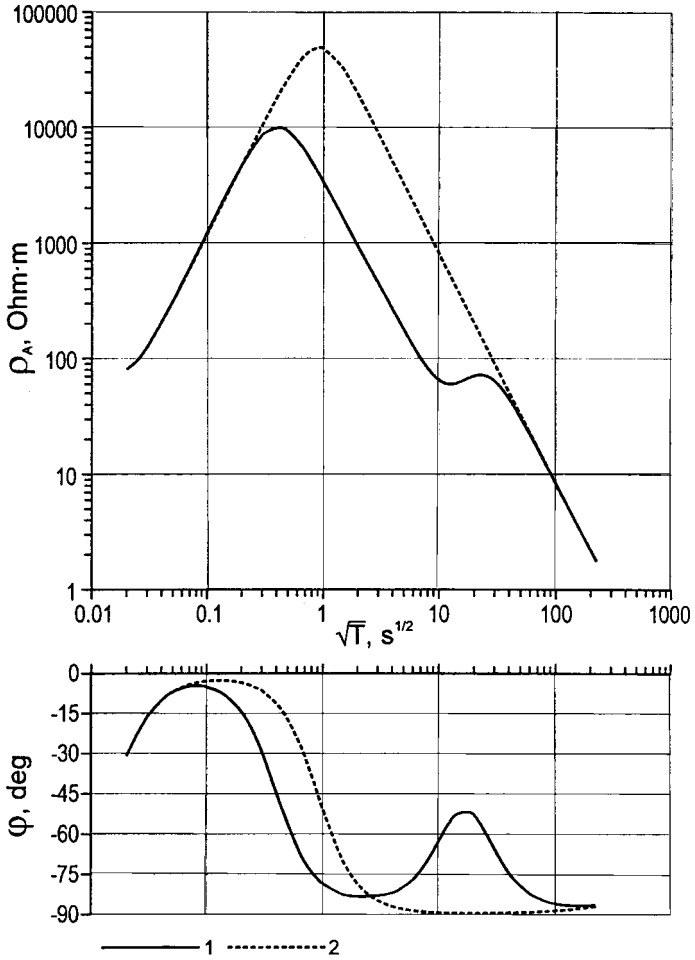

Figure 11. Apparent resistivity and impedance phase curves calculated from longitudinal and transverse components of the 2D regional impedance, for model B in Figure 3. 1 — longitudinal curve (the TE mode), 2 – transverse curve (the TM mode).

Z]. The local-regional decomposition is stable, providing that Δ is much greater than the errors of phase measurements.

The parameter q is the normalized Frobenius norm of the magnetic distortion matrix defining the contribution of the local magnetic anomaly:

$$q = \sqrt{\frac{|h_{xx} - 1|^2 + |h_{xy}|^2 + |h_{yx}|^2 + |h_{yy} - 1|^2}{2}}. \tag{20}$$

We can neglect the magnetic anomaly and apply basic Equation (18), providing that q is sufficiently small.

The parameter

$$\text{skew} = \left| \frac{Z_{xx} + Z_{yy}}{Z_{xy} - Z_{yx}} \right| \tag{21}$$

indicates a departure from the two-dimensionality or axial symmetry. In 2D models skew = 0.

The parameter

$$\eta = \frac{\sqrt{|\text{Im}(Z_{xy} Z_{yy}^* + Z_{xx} Z_{yx}^*)|}}{|Z_{xy} - Z_{yx}|} \tag{22}$$

with the asterisk denoting the complex conjugate is the phase-sensitive skew. At frequencies reflecting the regional structure this parameter indicates the adequacy of the 2D + 3D superposition model and applicability of basic Equation (18). The favorable indication is $\eta < 0.1$.

All these parameters are shown in Figure 12.

At T > 2 s the phase-sensitive skew η reaches the level of 0.1 and tends to zero indicating the feasibility of the local-regional decomposition. Small η-values correlate with a drop in q, which is an indication of the attenuation of magnetic distortions.. Within this frequency range we choose the area FA with $\Delta > 7.5°$, which is most favorable for the local-regional decomposition. It is notable that skew $\gg \eta$ over a wide range of periods. This has a simple explanation. While skew characterizes the general asymmetry of the medium, the phase-sensitive skew η manifests the symmetry of the regional 2D structure.

Figure 13 presents the results of the Bahr decomposition, which has been carried out against random noises with standard deviation of 5% in the impedance amplitudes and 3° in the impedance phases. Within the favorable area FA we determine the strike α of the regional 2D structure and the phases φ of the regional 2D impedances with sufficient accuracy. The similar results have been obtained by the Groom-Bailey decomposition, even with a slightly higher accuracy (Figure 14). The necessity of frequency restrictions taking into account the phase difference Δ is clearly seen in determining the twist β_T and shear β_S angles (Figure 15). Here the scatter in the results of the Groom-Bailey decomposition outside of the favorable area FA dramatically increases.

Evidently the *local-regional decomposition should be preceded by analysis of* η, *skew*, Δ *and detection of favorable frequency range.*

6. On the Sensitivity of the TM and TE Models

Figure 16 shows a model with a 2D narrow horst-like resistive elevation in the upper layer (sediments). This shallow structure is clearly marked by all graphs of

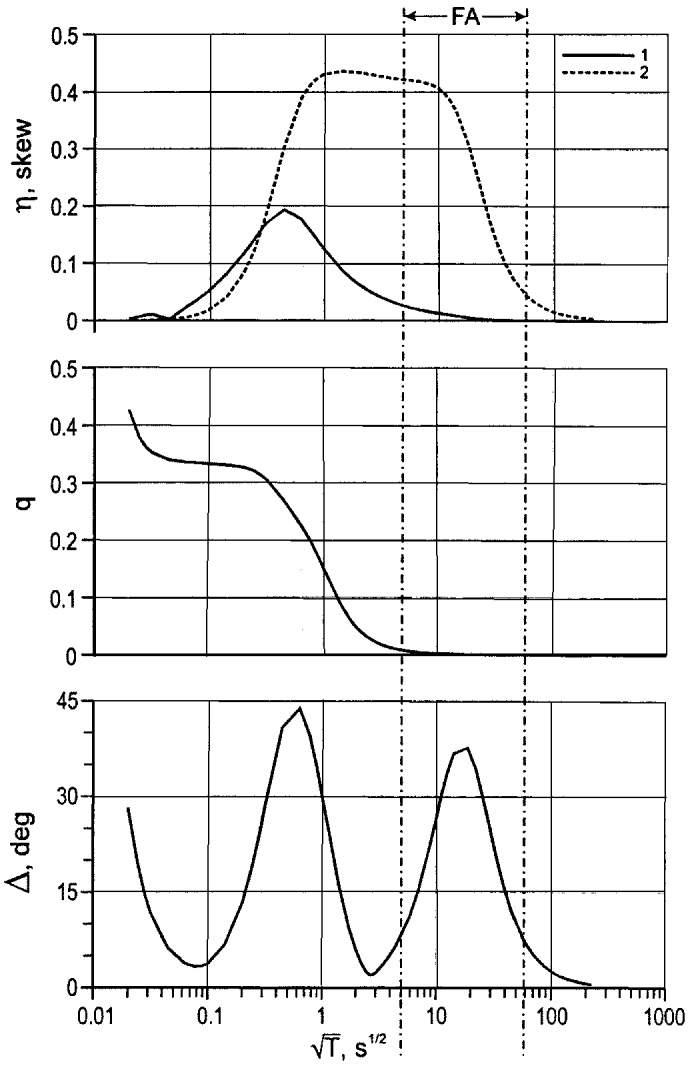

Figure 12. Characteristic parameters η, skew, q, and Δ for model B in Figure 3. FA – favorable area. Uppermost graph: 1 – η, 2 – skew.

the transverse apparent resistivity (the TM mode) calculated for periods from 0.1 to 10 000 s, but it is barely perceptible in the corresponding graphs of the longitudinal apparent resistivity (the TE mode).

Figure 17 shows a model with the uniform upper layer and a broad trapezoidal elevation of the conductive asthenosphere. This deep structure is clearly marked by low-frequency graphs of the longitudinal apparent resistivity (the TE mode, T = 100, 1000, 10 000 s), but it is not reflected in any of the graphs of the transverse

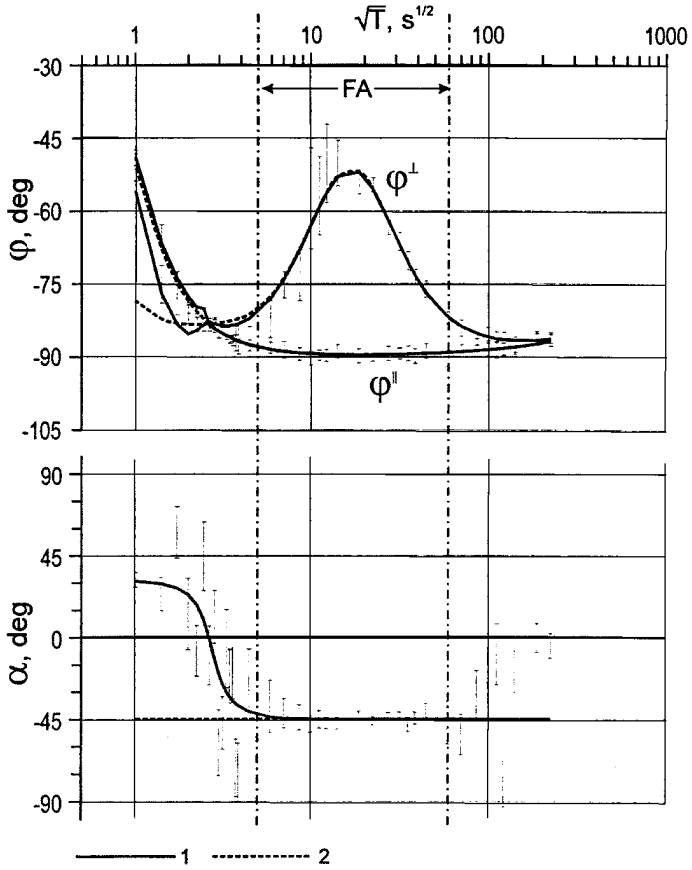

Figure 13. The Bahr decomposition: regional strike α and longitudinal $\varphi^{\parallel}$ and transverse $\varphi^{\perp}$ phases of the 2D regional impedance; vertical bars characterize the data scattering caused by noise in the local impedance, FA – favorable area, for model B in Figure 3. 1 – data for the noise-free local impedance, 2 – true data.

apparent resistivity (the TM mode, T = 0.1 $\sim$ 10 000 s, the intensive screening by the high-ohmic lithosphere).

Thus, *the TM impedance is more sensitive to shallow (resistive) structures and resistance of the high-ohmic lithosphere, but the TE impedance is more sensitive to deep (conductive) structures.*

7. On the Robustness of the TM and TE Modes

First we study the model, which is similar to that examined by Wannamaker, Hohman and Ward (1984). The model is shown in Figure 18. The apparent resistivity curves obtained for a conductive 3D prism (ρ_P = 2 Ohm.m) are presented at the

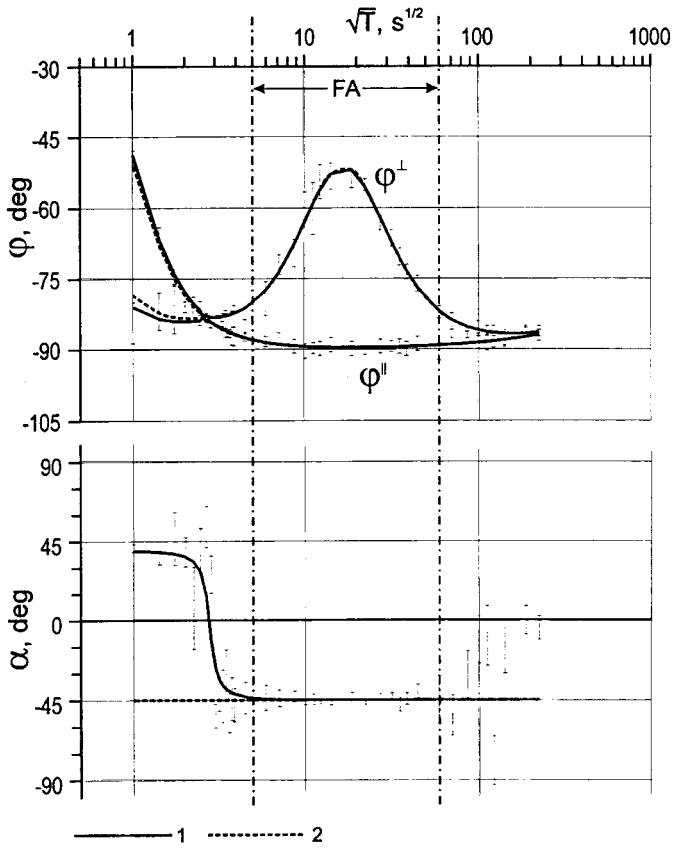

Figure 14. The Groom–Bailey decomposition: regional strike α and longitudinal $\varphi^{\parallel}$ and transverse $\varphi^{\perp}$ phases of the 2D regional impedance; vertical bars characterize the data scattering caused by noise in the local impedance, FA – favorable area, for model B in Figure 3. 1 – data for the noise-free local impedance, 2 – true data.

left panel of Figure 19. Here the transverse ρ_A-curve (T) oriented across the 3D prism is close to the ρ_A-curve corresponding to the TM mode in the associated 2D model. At the same time, the longitudinal ρ_A-curve (L) oriented along the 3D prism differs drastically from the ρ_A-curve corresponding to the TE mode in the associated 2D model. So, the two-dimensional inversion is sufficiently accurate with the transverse MT-curves, but can give crazy artifacts with the longitudinal MT-curves. This modeling result seems to be very impressive. The illusion appears that "the TM impedance should be preferable for 2D inversion since it is more robust to 3D effects than the TE impedance".

Now we substitute a resistive 3D prism (ρ_p = 40 000 Ohm.m) for a conductive one. Here we obtain the apparent resistivity curves shown at the right panel of Figure 19. We see that the relations change radically: in the 3D model with a resistive prism the longitudinal ρ_A-curve as well as the transverse ρ_A-curve are

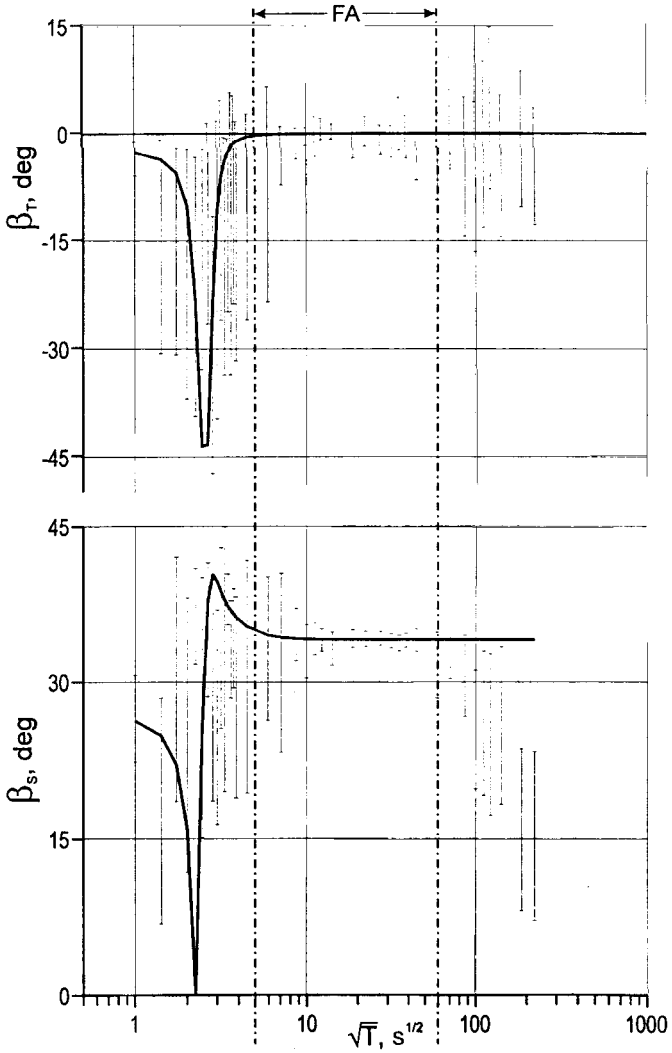

Figure 15. The Groom–Bailey decomposition: twist-angle β_T and shear-angle β_S; vertical bars characterize the data scattering caused by noise in the local impedance, FA – favorable area, for model B in Figure 3. Solid line – data for the noise-free local impedance.

close to the ρ_A-curves corresponding to the TE and TM modes in the associated 2D model. In this case the TM and TE impedances are equally robust to 3D effects. Moreover, it is easy to construct a model where the TE impedance is much more robust to 3D effects than the TM impedance. As an example, Figure 20 shows the model with a 3D resistive horst. Consider the ρ_A-curves obtained at sites A, B, C, which are 5, 3, and 1 km from the horst (Figure 21). At all these sites the longitudinal ρ_A-curves are close to their TE counterparts. But the transverse ρ_A-curves are dramatically distorted by the around-flow effects. They diverge from

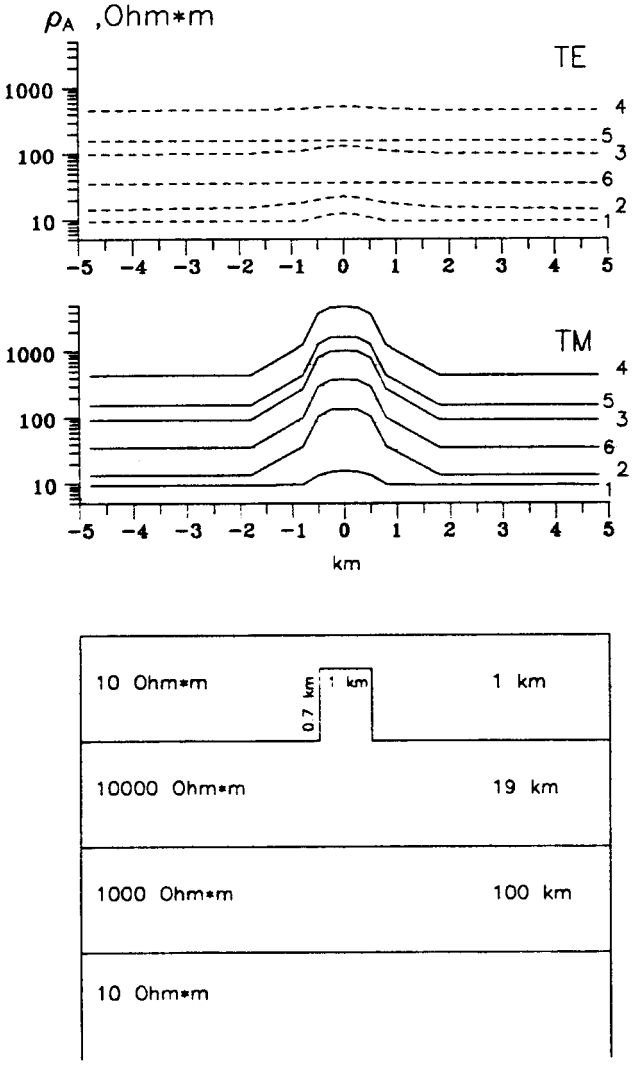

Figure 16. Model with a two-dimensional horst-like resistive elevation in the sedimentary cover. At the bottom: the model cross-section (not to scale). At the top: the apparent resistivity profiles for the TE and TM-modes, profile parameter: period T, 1–0.1 s, 2–1 s, 3–10 s, 4–100 s, 5–1000 s, 6–10 000 s; taken from Berdichevsky et al. (1998).

their TM counterparts and near the horst tip over (here the degree of distortion of the transverse ρ_A-curve is almost the same as in the case of the longitudinal ρ_A-curve in the model with a conductive prism). It is clear that the wording "the TM impedance is more robust to 3D effects than the TE impedance" (Wannamaker et al., 1989) should be edited. We have to say that "*the TM impedance is more robust to 3D effects caused by conductive structures (that is, by current gathering), but*

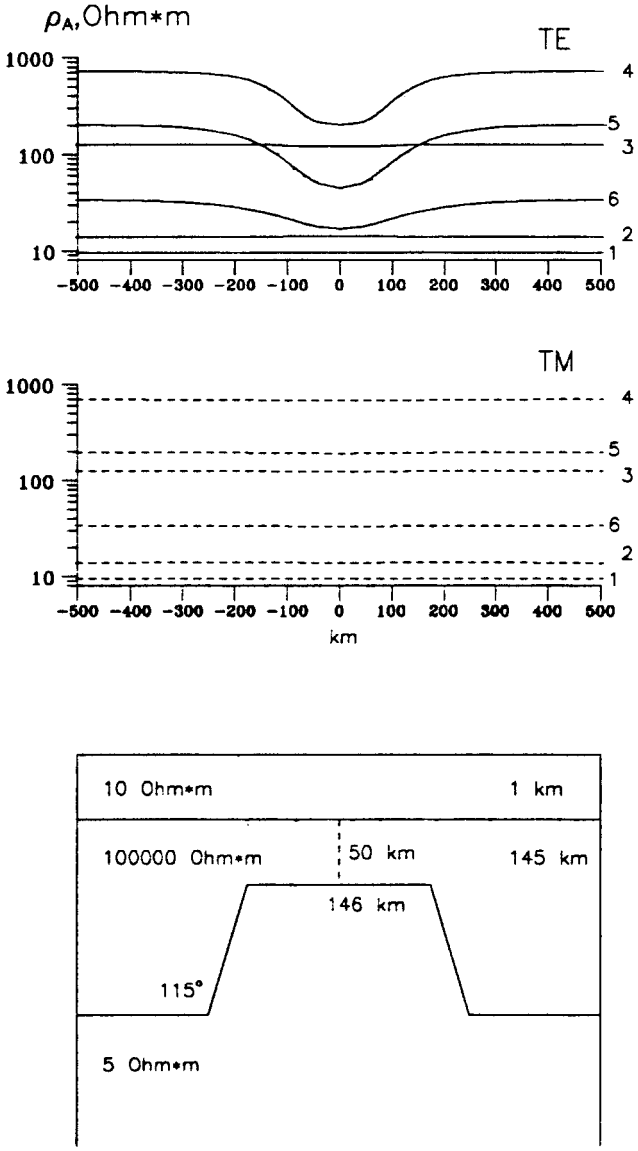

Figure 17. Model with a two-dimensional elevation of the conductive asthenosphere. At the bottom: the model cross-section (not to scale). At the top: the apparent resistivity profiles for TE and TM-modes, profile pararameter: period T, 1 – 0.1 s, 2 – 1 s, 3 – 10 s, 4 – 100 s, 5 – 1000 s, 6 – 10 000 s; taken from Berdichevsky et al. (1998).

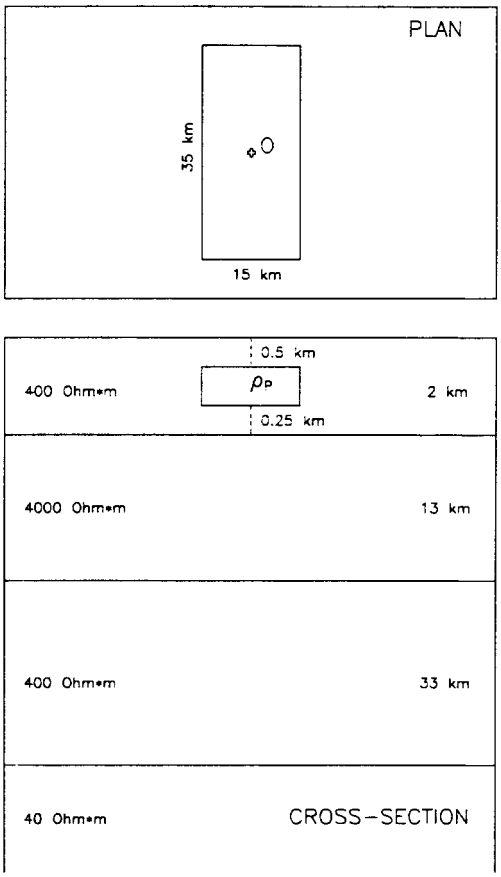

Figure 18. Model with a three-dimensional elongated prism of resistivity ρ_p in the first layer (not to scale), O-observation site; taken from Berdichevsky et al. (1998).

the TE impedance may be more robust to 3D effects caused by resistive structures (that is, by current around-flow)".

Finally I give a field example, which confirms this consideration. Figure 22 presents MT-curves that have been obtained along a profile crossing the Precaucasian foredeep. The profile is 150 km long and its southern end lies on the foot of the Caucasian ridge. It is remarkable that the longitudinal ρ_A-curves are almost undistorted, and their 2D inversion gives the relief of the crystalline basement which correlates with seismics and drilling data. But the transverse ρ_A-curves are dramatically distorted by intense around-flow effects (currents flow around the high-ohmic Caucasian Ridge). Their 2D inversion is senseless.

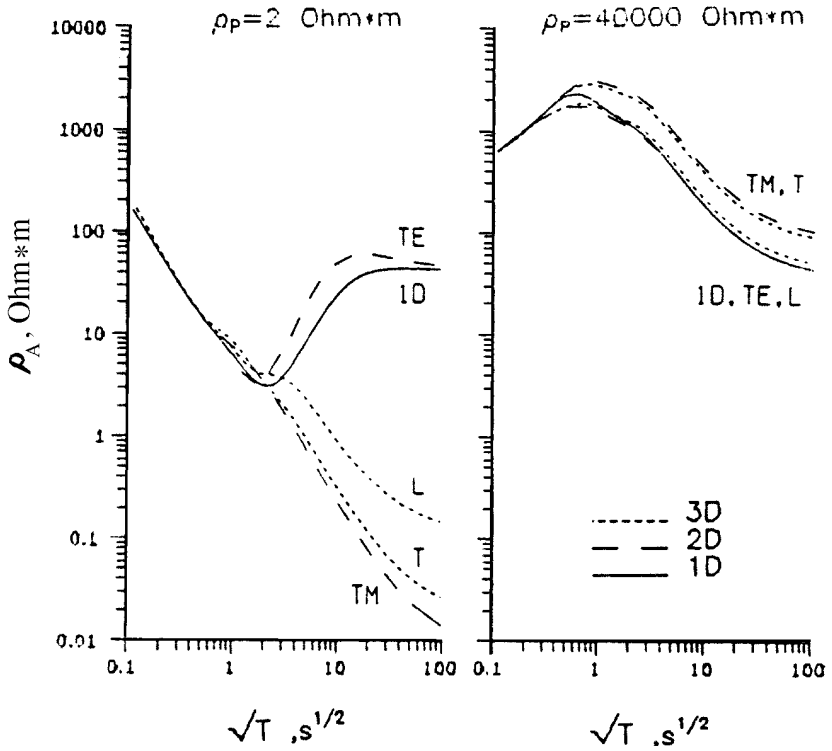

Figure 19. Apparent resistivity curves at site O for a model with a three-dimensional elongated prism of resistivity ρ_p (see Figure 18). Solid line: 1D-curves. Dashed line – long dash: 2D-curves for TE and TM modes, short dash: 3D-curves for longitudinal (L) and transverse (T) polarization of the electric field; taken from Berdichevsky et al. (1998).

8. On the Static Shift

We have to discern two kinds of the static shift: (1) the ρ-effect caused by small near-surface inliers and (2) the S-effect caused by variations in the integral conductance S of the upper conductive layer (Berdichevsky, Dmitriev and Pozdnjakova 1998). The ρ- and S-effects are exemplified by Figure 23. In the ideal 2D model they act upon transverse ρ_A-curves and do not touch longitudinal ρ_A-curves. Behind both effects are the same galvanic mechanisms, but they operate in different frequency intervals. The ρ-effect shifts the ρ_A-curves in the wide frequency range (including their ascending and descending branches), while the S-effect shifts only low-frequency part of the ρ_A-curves and does not affect the ascending branch caused by the resistive bed that underlies the upper conductive layer. Both effects manifest the same conformal relations between the shifted and normal (remote) ρ_A-curves, and can be identified using the phase curves. The basic rule for static shift correction is simple: the ρ_A-curves should be corrected in the frequency range where phases change slightly along profile.

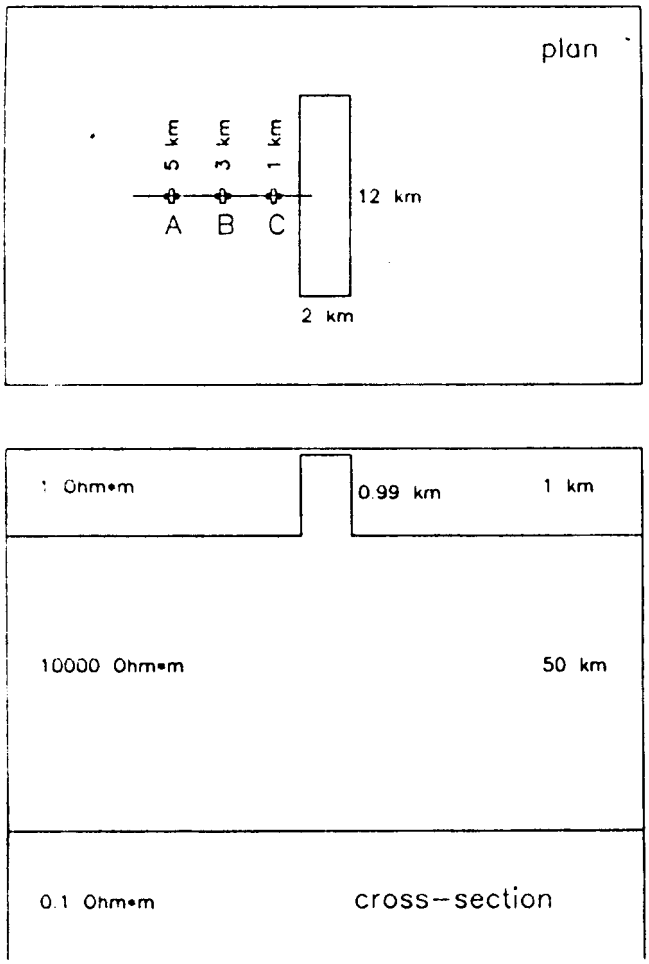

Figure 20. Model with a three-dimensional horst-like resistive elevation in the sedimentary cover (not to scale), A,B,C – observation sites and their distance to elevation edge; taken from Berdichevsky et al. (1998).

Note that in the vicinity of elongated structures the longitudinal ρ_A-curves inherit properties of the ideal TE mode and experience a far lesser static shift than the transverse ρ_A-curves do. The typical example is shown in Figure 24. Unfortunately, in actual practice, we may deal with superposition of elongated structures and local 3D-inhomogeneities, where not only transverse, but longitudinal apparent resistivity curves also suffer from the ρ- and S-effects.

Though the static shift changes neither the shape of long-period part of ρ_A-curves nor corresponding phases, it drastically plagues the interpretation of MT-data. Success of MT-interpretation depends greatly on reliability of the static shift corrections. I have to stress that there is no standard universal remedy for static shift

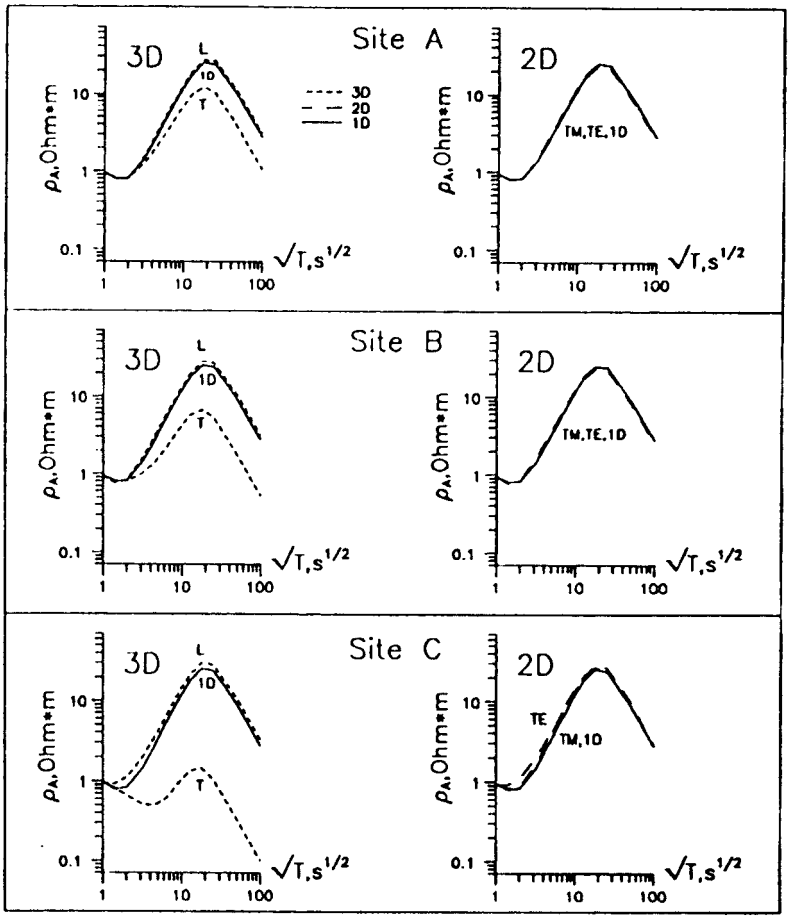

Figure 21. Apparent resistivity curves in the vicinity of a horst-like elevation (see Figure 20). MT-soundings at sites A,B,C. Solid line: 1D-curves. Dashed line – long dash: 2D-curves for TE and TM-modes, short dash: 3D-curves for longitudinal (L) and transverse (T) polarization of the electric field; taken from Berdichevsky et al. (1998).

– the best result can be attained by combining different correction techniques and controlling them by phase and tipper inversion, and independent geological and geophysical information. Modern magnitotellurics offers a number of methods for the static shift correction. These methods reduce to statistic averaging, filtering, displacement to some reference points, mathematical modelling. Overviews of popular shift correction methods have been given by Jones (1988), Berdichevsky et al. (1989), Pellerin and Hohmann (1990), Vozoff (1991), Zinger (1992), Berdichevsky et al. (1998).

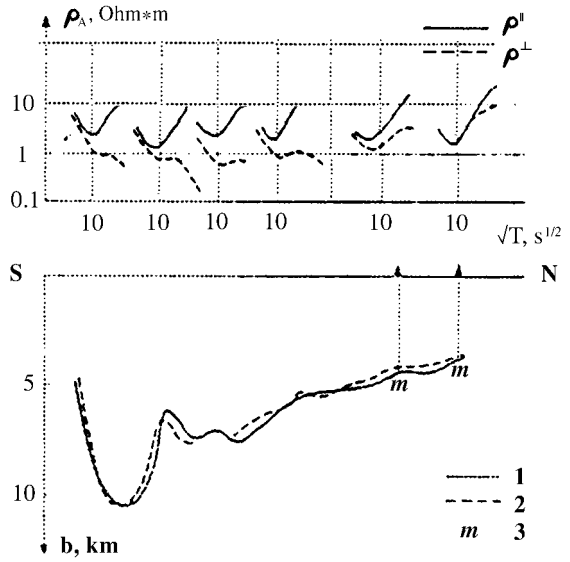

Figure 22. Longitudinal ($\rho^{\parallel}$) and transverse ($\rho^{\perp}$) apparent resistivity curves along profile crossing the Precaucasian foredeep (top) and geophysical cross-section (bottom), 1,2,3-surface of the Paleozoic basement: 1-from the $\rho^{\parallel}$-curves, 2-from seismics, 3-from drilling; taken from Berdichevsky et al. (1998).

9. On Strategy of the Two-Dimensional Interpretation

While the transverse MT curves provide higher accuracy in the 2D-approximation of conductive structures and higher sensitivity to near-surface structures and to the lithosphere resistance and deep faults, the longitudinal MT curves provide higher sensitivity to deep structures and may ensure higher accuracy in the 2D-approximation of resistive structures. And when the transverse ρ_A-curves suffer dramatically from the static shift, the longitudinal ρ_A-curves may be almost undistorted. The transverse and longitudinal MT curves nicely complement each other: gaps and shortcomings left by one mode are filled by another mode. In this sense one can say that *the TM and TE modes of the two-dimensional magnetotelluric field satisfy the principle of information complementarity.* The complementarity principle forms a sound basis for the two-dimensional interpretation strategy.

Generally, *the most reliable and comprehensive information on the Earth's conductivity can be obtained by means of the bimodal inversion of the MT data, using both modes.*

The international project EMSLAB gives the dramatic example of imperfection of the unimodal inversion. Figure 25 presents the two-dimensional resistivity cross-section through the Juan de Fuca subduction zone plotted with priority for the TM impedance, which, as the authors say, is "more robust to common deviations from two-dimensional assumption" (Wannamaker et al., 1989). The most inter-

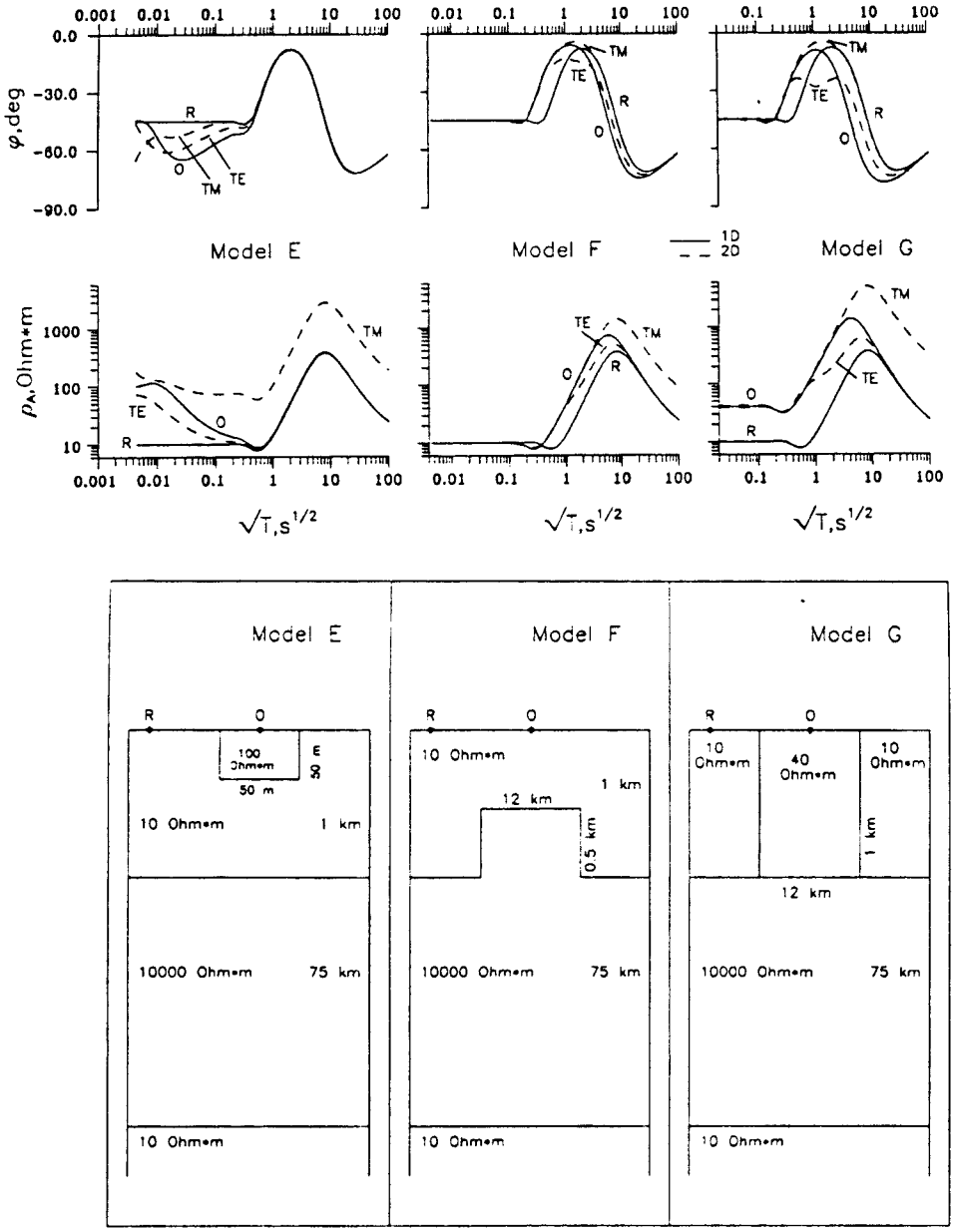

Figure 23. At the bottom: different inhomogeneities in the sedimentary cover. Model E: a local near-surface resistive inlier, model F: a horst-like elevation of resistive rocks, model G: an increase of sediment series resistivity, O,R – observation sites, the distance OR is 1 km (model E) and 50 km (models F,G). At the top: apparent resistivity and impedance phase curves in models E, F and G. Model E shows the ρ-effect, models F and G show the S-effect. Solid lines: 1D-curves at central site O and remote site R, dashed lines: 2D-curves for the TE and TM-modes at central site O; taken from Berdichevsky et al. (1998).

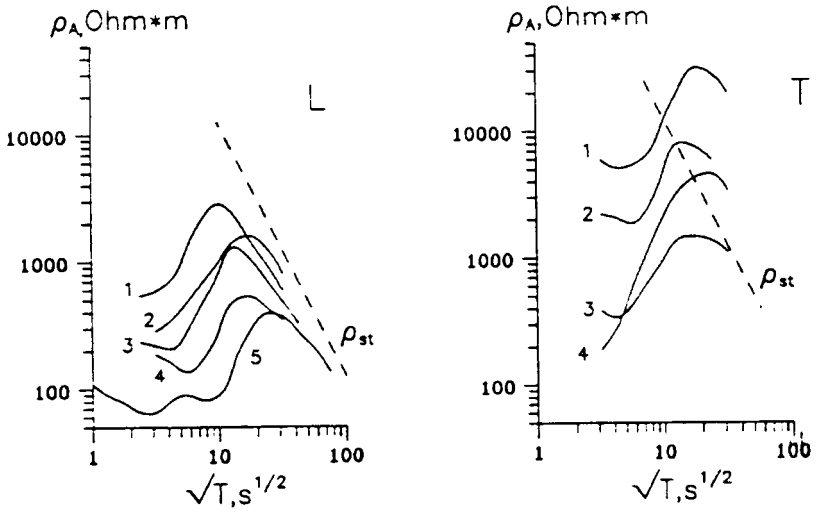

Figure 24. Longitudinal (L) and transverse (T) apparent resistivity curves characteristic of the Urals, ρ_{st} – the standard apparent resistivity curve based on the Clobal Magnetovariation Sounding and voluminous MTS statistics; taken from Dyakonova et al. (1986).

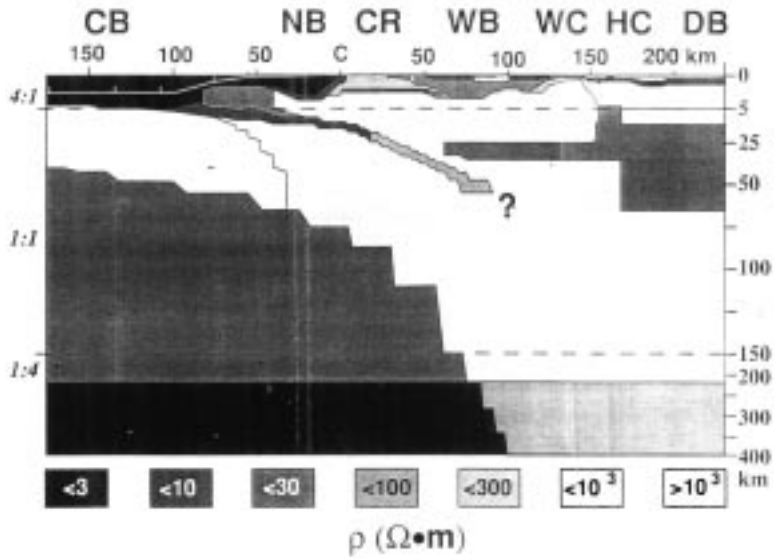

Figure 25. East–west resistivity cross-section through the Juan de Fuca subduction zone constructed from the unimodal MT-inversion (using the TM mode). CB – Cascadia Basin, NB – Newport Basin, CR – Coast Rang, WB – Willamette Basin, WC – Western Cascades, HC – High Cascades, DB – Deshutes Basin. The values of resistivity are indicated in Ohm.m; taken from Wannameker et al. (1989).

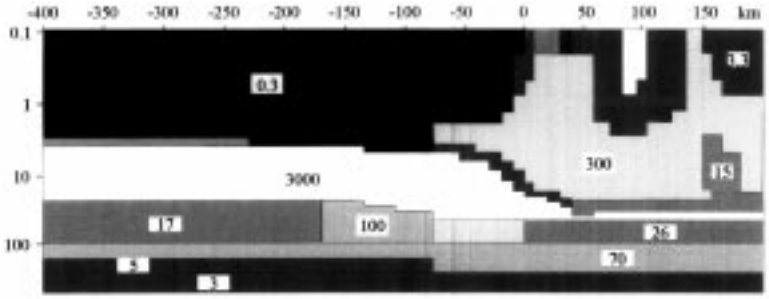

Figure 26. East–west resistivity cross-section through the Juan de Fuca subduction zone constructed from the bimodal MT-inversion (using the TM and TE modes). C – the coast. The values of resistivity are indicated in Ohm.m; taken from Varentsov et al. (1996).

esting features of this model are: (1) a low-resistivity subduction layer beneath the Coast Range, (2) a subhorizontal conductive layer in the continental middle crust, and (3) the well-developed conductive asthenosphere beneath the ocean and its degeneration and disappearance beneath the continent. Later analysis of the model showed that the sensitivity of the TM impedance to mantle conductivity is very poor (the screening effect) and only the TE impedance can give a clue to the study of the asthenosphere (Berdichevsky, Koldaev and Jakovlev, 1992). Figure 26 displays the result of the bimodal interpretation of EMSLAB data performed by Russian geophysicists (Varentsov et al., 1996). Inversion has been carried out by Tikhonov's regularized minimization of model misfit involving (1) phases of the TM impedance and real parts of the tipper (maximum weight), (2) phases of the TE impedance and transverse apparent resistivities (normal weight), and (3) longitudinal apparent resistivities (minimum weight). The upper part of Varentsov's model is in gratifying agreement with Wannamaker's model. The main distinctive element of the Varentsov model is a continental conductive layer at a depth of 50 km, which can be identified with the partially melted asthenosphere. It hardly needs to be stated that the new data for the continental asthenosphere change our idea of geodynamics and thermodynamics of the subduction zone.

Acknowledgements

My deep gratitude is to J. Weaver for encouraging me to publish these fragmentary notes and to the reviewers, P. Kaikkonen and K.V. Paulson, for their constructive and benevolent comments, which helped me in preparing the paper.

The work was supported by RFBR, Project 99-05-64758.

References

Bahr, K.: 1988, Interpretation of magnetotelluric impedance tensor: Regional induction and local telluric distortion, *J. Geophys.* **62**, 119–127.

Berdichevsky, M. N. and Dmitriev, V.I.: 1976, Basic principles of interpretation of magnetotelluric sounding curves, in monograph "Geoelectric and Geothermal Studies", Akademiai Kiado, Budapest.

Berdichevsky, M.N., Vanyan, L.L., and Dmitriev, V.I.: 1989, Methods used in the USSR to reduce near-surface inhomogeneity effects on deep magnetotelluric soundings, *Physics of the Earth and Planetary Interiors* **53**, 194–206.

Berdichevsky, M.N., Koldaev, D.S., and Jakovlev, A.G.: 1992, Magnetotelluric sounding on the ocean coast, Izv. Acad. Nauk SSSR, Fiz. Zemli, No. 6, 87–96.

Berdichevsky, M.N. and Dmitriev, V.I.: 1997, On deterministic nature of magnetotelluric impedance, *Acta Geophysica Polonica* **XLV**(3), 227–236.

Berdichevsky, M.N. and Pokhotelov, D.O.: 1997a, Dispersion relations in terms of a polarized medium, *Physics of the Solid Earth* **33**(7), 539–542.

Berdichevsky, M.N. and Pokhotelov, D.O.: 1997b, Violation of the dispersion relations in a three-dimensional magnetotellutic model, *Physics of the Solid Earth* **33**(8), 603–612.

Berdichevsky, M.N., Dmitriev, V.I. and Pozdnjakova, E.E.: 1998, On two-dimensional interpretation of magnetotelluric soundings, *Geophys. J. Int* **133**, 585–606.

Debabov, A.S.: 1980, On modelling of electromagnetic fields for heterogeneous media, *DAN SSSR* **250**(2), 326–331.

Dyakonova, A.G., Ingerov, A.I., and Rokityansky, I.I.: 1986, *Electromagnetic Soundings on the Eastern European Platform and in the Urals*, Naukova Dumka, Kiev.

Egbert, G.: 1990, Comments on "concerning dispersion relations for the magnetotelluric impedance tensor" by E. Yee and K. Paulson, *Geophys. J. Int* **102**, 1–8.

Eggers, D.E.: 1982, An eigenstate formulation of the magnetotelluric impedance tensor, *Geophysics* **47**, 1204–1214.

Fischer, G. and Schnegg, P.: 1980, The dispersion relations of the magnetotelluric response and their incidence on inverse problem, *Geophys. J.R. Astr. Soc.* **62**, 661–673.

Fischer, G. and Schnegg, P.: 1993, The magnetotelluric dispersion relations over 2-D structures, *Geophys. J. Int.* **115**, 1119–1123.

Groom, R.W. and Bailey, R.C.: 1989, Decomposition of magnetotelluric impedance tencors in the presence of local three-dimensional galvanic distortion, *J. Geophys. Res.* **94**(B2), 1913–1925.

Jones, A. G.: 1988, Static shift of magnetotelluric data and its removal in a sedimentary basin enviroment, *Geophysics* **53**(7), 967–978.

LaTorraca, G.A., Madden, T.E., and Korringa, J.: 1986, An analysis of magnetotelluric impedance for three-dimensional conductivity structures, *Geophysics* **51**(9), 1819–1829.

Pellerin, L. and Hohman, G.W.: 1990, Transient electromagnetic inversion: A remedy for magnetotelluric static shift, *Geophysics* **55**(9), 1242–1250.

Sims, W.E. and Bostick, F.X.: 1967, Methods of magnetotelluric analysis, Tech. rep. 58, Electr. Geophys. Res. Lab., Univ. of Texas.

Svetov, B.S.: 1991, Transfer functions of the electromagnetic field, Izv. Acad. Nauk SSSR, Fiz. Zemli, No. 1, 119–128.

Swift, C.M.: 1967, A magnetotelluric investigation of an electrical conductivity anomaly in the southwestern United States, Ph.D., MIT, Cambridge.

Torres-Verdin, C. and Bostick, F. X.: 1992, Principles of spatial surface electric field filtering in magnetotellurics: Electromagnetic array profiling, *Geophysics* **57**, 603–622.

Varentsov, I.M., Golubev, N.G., Gordienko, V.V., and Sokolova, E.J.: 1996, Study of deep geoelectrical structure along Lincoln line (project EMSLAB), Izv. Acad. Nauk SSSR, Fiz. Zemli, No. 4, 124–144.

Wannamaker, P.E., Booker, J.R., Jones, A.G., Chave, A.D., Filloux, J. H., and Waff, H.S., and Law, L.K.: 1989, Resistivity cross-section through the Juan de Fuca subduction system and its tectonic implication, *J. Geophys. Res.* **94**(B10), 14127–14144.

Wannamaker, P.E., Hohman, G.W., and Ward, S.H.: 1984, Magnetotelluric responses of three-dimensional bodies in layered earth, *Geophysics* **49**(9), 1517–1533.

Wannamaker, P.E., Stodt, J.A., and Rijo, L.: 1987, A stable finite element solution for two-dimensional magnetotelluric modelling, *Geophys. J.R. astr. Soc.* **88**, 277–296.

Weidelt, P.: 1972, The inverse problem of geomagnetic induction, *Zeitschrift fur Geophysik* **8**(2), 257–290.

Weidelt, P. and Kaikkonen, P.: 1994, Local 1-D interpretation of magnetotelluric B-polarization impedance, *Geophys. J. Int.* **117**, 733–748.

Yee, E. and Paulson, K.: 1987, The canonical decomposition and its relationships to other forms of magnetotelluric impedance tensor analysis, *J. Geophys. 61*, 173–189.

Yee, E. and Paulson, K.: 1988, Concerning dispersion relations for the magnetotelluric impedance tensor, *Geophys. J.* **95**, 549–559.

Vozoff, K.: 1991, The magnetotelluric method, in monograph "Electromagnetic Methods in Applied Geophysics-Applications", vol. 2, Soc. Explor. Geophys., Tulsa.

Zinger, B.Sh.: 1992, Correction for distortions of magnetotelluric fields: limits of validity and static approach, *Surveys in Geophysics* **13**, 309–340.